



Influence of region-dependent error growth on the predictability of track and intensity of Typhoon Chan-hom (2020) in high-resolution HWRF ensembles



Jie Feng ^{a,b}, Falko Judt ^c, Jing Zhang ^{d,*}, Xuguang Wang ^e

^a Department of Atmospheric and Oceanic Sciences and Institute of Atmospheric Sciences, Fudan University, Shanghai, China

^b Shanghai Key Laboratory of Ocean-land-atmosphere Boundary Dynamics and Climate Change, Fudan University, Shanghai, China

^c Mesoscale and Microscale Meteorology Laboratory, National Center for Atmospheric Research, Boulder, CO, USA

^d Shanghai Typhoon Institute, China Meteorological Administration, Shanghai, China

^e School of Meteorology, University of Oklahoma, Norman, OK, USA

ARTICLE INFO

Keywords:

Tropical cyclone

Predictability

Multi-scale error growth

ABSTRACT

Enhancing the predictive capabilities for tropical cyclones (TCs) necessitates comprehensive investigations into their predictability. This study employs convection-allowing ensemble forecasts using the Hurricane Weather Research and Forecasting model, integrating perturbed initial conditions to examine error growth and initial condition error-related predictability (IE-predictability) of TCs. Distinctively, our research concentrates on how the predictability of TC track and intensity is influenced by initial errors in various zones: (1) the inner core and outer rainbands (0–350 km), (2) the near environment (350–1300 km), and (3) the far environment (1300–3500 km).

Contrary to many prior studies, our findings suggest that the most critical region for initial errors affecting TC track forecasts is within the TC inner structures. For Typhoon Chan-hom (2020), characterized by significant track forecast discrepancies, the initial inaccuracies in the inner core and outer rainbands substantially affect the TC's proximate environment and track, more so than errors in the near and far environments. Regarding TC intensity, the inner core emerges as the most sensitive area. The surface wind configuration of the TC inner core at larger scales (wavenumbers 0–2) maintains predictability for over three days, whereas its structure at finer scales is only predictable for a few hours.

Plain language summary: The forecasting of tropical cyclones (TCs) has seen significant advancements over recent decades. A critical question arises: to what extent can we further enhance the accuracy of TC predictions? Addressing this requires in-depth exploration of TC predictability. In our study, we utilized convection-allowing ensemble forecasts based on the Hurricane Weather Research and Forecasting (HWRF) model, incorporating perturbed initial conditions to analyze the development of forecast errors and the predictability related to these initial errors in TCs. A novel aspect of this research is its emphasis on the impact of initial errors in different regions on the predictability of TC track and intensity. Our key findings are twofold: (1) The region most impacted by initial errors for TC track predictions may not always be the surrounding environment. Instead, errors within the TC's inner core and outer rainbands, owing to their pronounced interplay, can lead to significantly greater track forecast errors compared to those in the near and far environments. (2) As for TC intensity, the inner core emerges as the most susceptible region. The large-scale components (wavenumbers 0–2) of the TC's inherent vortex flow can be forecasted accurately for over four days, largely due to the predictability of the synoptic-scale environment. In contrast, the smaller-scale components (wavenumbers >2) demonstrate predictability for only a few hours.

* Corresponding author.

E-mail address: zhang@typhoon.org.cn (J. Zhang).

1. Introduction

The accurate prediction of tropical cyclones (TCs) remains challenging, even with recent advancements in theoretical understanding, enhanced observing systems, improved numerical models, and refined data assimilation techniques. A critical aspect of these predictions is the intensity of TCs, which serves as a key indicator of their potential for destruction. Predicting this intensity is particularly challenging due to the intricate interactions across phenomena at different scales within TCs (Wang and Wu, 2004; Gopalakrishnan et al., 2011). Notably, the accuracy of TC intensity forecasts has improved only marginally over the past decades, as documented by Cangialosi and Franklin (2014), DeMaria et al. (2014), Emanuel and Zhang (2016), and Cangialosi et al. (2020). In contrast, the accuracy in forecasting TC tracks has seen a more significant improvement, with errors decreasing by over 50 % in the same timeframe (Katz and Murphy, 2015; Cangialosi et al., 2020). However, despite these advances, substantial errors still persist in predicting the tracks of TCs, particularly for those exhibiting curving, looping, or stalling trajectories (Wu et al., 2014; Torn et al., 2015; Feng et al., 2022). This limited progress in further reducing errors in TC track and intensity forecasts raises fundamental questions about their inherent predictability.

The trajectory of a TC is predominantly influenced by the large-scale environmental steering flow, as corroborated by various studies (Emanuel et al., 2004; Wu et al., 2005). This steering flow encompasses the weather systems surrounding a TC, including the monsoon trough, the subtropical ridge, and the mid-latitude trough (Chia and Ropelewski, 2002; Wu et al., 2005). From predictability perspective, many researches indicate that inaccuracies in the structures and positions of these synoptic-scale systems due to the deficiencies in data assimilation and model configuration are a primary source of errors in TC track predictions (Ito and Wu, 2013; Torn et al., 2018; Ashcroft et al., 2021; Hazelton et al., 2023; Qin et al., 2023; Zhang et al., 2023). For instance, Nystrom et al. (2018) demonstrated that the most significant track prediction errors for Hurricane Joaquin in 2015 originated from the environmental region extending beyond 300 km from the TC's center, as determined through ensemble-based sensitivity analysis. In contrast, there are relatively fewer investigations suggesting that errors stemming from internal TC processes can significantly alter the TC's surrounding environment. Such alterations, driven by mechanisms like the advection of potential vorticity, can subsequently lead to deviations in the TC's trajectory (Torn et al., 2015). Nevertheless, there remains a lack of consensus regarding which region of initial condition errors is most critical for accurate track forecasting.

Forecasting the intensity of TCs is notably more complex than predicting their track, owing to the intricate interplay of dynamic and thermodynamic processes across various spatiotemporal scales (Wang and Wu, 2004; Gopalakrishnan et al., 2011). Specifically, extensive research over decades has established that the large-scale environmental factors, such as vertical wind shear, significantly influence TC intensity (Black et al., 2002; Chen et al., 2006; Tang and Emanuel, 2012; Rios-Berrios and Torn, 2017). Additionally, the temperature and salinity of the upper ocean (Emanuel et al., 2004) and the dynamics of air-sea interactions are crucial (Emanuel, 1986; Chen et al., 2007, 2013; Ma et al., 2017, 2018). Beyond these environmental influences, the role of internal mesoscale processes, which include moisture convective dynamics, eyewall replacement cycles, and potential vorticity anomalies, is also significant in determining TC intensity (Shapiro and Willoughby, 1982; Rogers, 2010; Zhang and Chen, 2012; Kutty and Gohil, 2017; Qin et al., 2021, 2023). Based on a perfect model framework, Emanuel and Zhang (2016) demonstrated the errors in initial storm intensity dominates the error growth of intensity forecasts over the first few days and then influence of the errors in the large-scale environment becomes pronounced. In addition, the complex interaction between the internal dynamics of TCs and their environmental conditions, particularly in relation to the evolution of spiral rainbands and secondary circulation,

has been thoroughly researched (Houze et al., 2006; Judt and Chen, 2010; Li and Wang, 2012). This intricate interplay poses significant challenges in accurately forecasting changes in TC intensity. A key aspect of enhancing predictability involves identifying specific regions where these physical processes have the most profound impact on TC intensity. Furthermore, the predictability of TC intensity is often assessed by evaluating how sensitive the predictions of TC intensity and structure are to variations in the initial conditions, i.e., the ensemble-based sensitivity analysis (e.g., Torn and Hakim, 2008; Ito and Wu, 2013; Ren et al., 2019; Jayakrishnan et al., 2020).

The ensemble-based approach has been widely used to understand the predictability of TC intensity forecasts. Sippel and Zhang (2008, 2010) demonstrated that initial errors in moist convection, even those of minimal magnitude, can escalate rapidly, influencing larger-scale physical processes through upscale error growth, which in turn limits the predictability of TC intensity. Complementing this, Van Sang et al. (2008) and Shin and Smith (2008) observed that minor initial random perturbations in boundary layer moisture can induce strong asymmetries in the TC vortex, leading to significant variability in intensity predictions. Beyond the impact of the TC inner core processes alone, studies by Zhang and Tao (2013), Tao and Zhang (2015), and Finocchio and Majumdar (2017) indicate that the predictability of TC intensity is further reduced (i.e., becomes more sensitive to initial uncertainties) in the presence of increased vertical wind shear. Judt and Chen (2016) identified that the intricate interplay among vertical wind shear, the mean vortex, and internal convective processes collectively contributes to the uncertainty in TC intensity forecasts. Despite extensive research into the sensitivity of TC intensity to various factors, the relative impact of initial errors in different regions on TC intensity predictions has not been explicitly addressed.

Several studies have attempted to quantify the upper limit of predictability for TC intensity. Kieu and Moon (2016) observed that the sample-mean forecast errors for TC intensity, as measured by the maximum sustained surface wind (MSW) speed, tend to stabilize at approximately $8\text{--}10 \text{ m s}^{-1}$ in both an axisymmetrical model and real-time data analysis. This observation led them to suggest a maximum predictability limit of around three days for MSW. Similarly, Hakim (2013) derived a comparable three-day predictability limit for the azimuthal wind in TCs, using analog forecasts based on extensive simulation data from an idealized axisymmetrical model. In a more focused study, Kieu and Rotunno (2022) reported that in an idealized TC simulation, the spectral kinetic error growth for high azimuthal wave-numbers reaches a saturation point after approximately nine hours, compared to about 18 h for the radial direction. Additionally, Zhong et al. (2018) estimated the predictability of TC intensity in the western North Pacific basin to range between two and a half to seven days, using a local dynamic analog method. However, it is important to note that these results are based on simplified TC models or algorithms within an ideal framework, and do not fully account for the effects of multi-scale physical processes on changes in TC intensity.

Judit et al. (2016) conducted a scale-dependent analysis of the predictability limits of the inner core surface winds in TCs using the cloud-resolving Weather Research and Forecasting (WRF) model and Fourier decomposition. Their findings revealed a clear scale-dependency in the error growth and predictability limits of surface wind speed: (1) the mean vortex and wavenumber-1 asymmetry exhibited predictability exceeding seven days; (2) the scales corresponding to rain bands (wavenumbers 2–5) maintained predictability for several days; and (3) convective scales (wavenumbers >7) demonstrated predictability only within a 6–12 h window. However, it is important to note that Judt et al. (2016) employed a stochastic perturbation method to mimic model error, involving continuous perturbation of the model fields. This methodology precluded a comprehensive assessment of the initial error-related predictability (IE-predictability) of TCs. IE-predictability refers to the potential for prediction accuracy when an almost perfect procedure is utilized, as explored in foundational studies by Lorenz (1969),

Sun and Zhang (2016), and Selz (2019).

Addressing the aforementioned limitations, this study focuses on exploring the IE-predictability of TC track and intensity. This investigation utilizes convection-allowing ensemble forecasts, employing perturbed initial conditions within the framework of the Hurricane Weather Research and Forecasting (HWRF) model. The HWRF model is a Non-Hydrostatic Mesoscale Model on the E Grid (NMM-E) and employs a suite of advanced physical parameterizations developed for TC applications (Biswas, 2018). Its application extends broadly within the area of data assimilation, prediction, and mechanism of TCs at operational and research centers (e.g., Zhang et al., 2016; Lu et al., 2017). A key objective of this study is to evaluate the different sensitivity of TC track and intensity forecasts to initial errors originating from distinct regions. To this end, we conducted a detailed analysis of error growth and the dynamics associated with these region-specific errors. The study specifically examines Typhoon Chan-hom in 2020, which exhibited significant uncertainties in both its track and intensity forecasts, thereby providing a pertinent case for analysis. This approach aims to enhance the understanding of how variations in initial conditions impact TC forecast accuracy, with a particular emphasis on the spatial attributes of these initial errors.

This paper is organized as follows. Section 2 describes the model setup. Section 3 provides a brief review of the typhoon case and introduces the experimental design. The results of the IE-predictability analysis are presented and discussed in Sections 4 (track) and 5 (intensity). Section 6 discusses the results of the combined effect of the initial and boundary uncertainties on the TC predictability. Finally, Section 7 presents our conclusions and discussion.

2. Model setup

The ensemble forecasts employed in our predictability analysis were produced using the most recent version of the regional high-resolution HWRF model (version 4.0a). The HWRF model is renowned for its application in both operational forecasting and academic research of tropical storms, as evidenced by studies such as those by Lu et al. (2017), Zhang et al. (2016, 2017, 2018), and Feng et al. (Feng and Wang, 2019; Feng and Wang, 2021). This model is configured with triply two-way nested domains to optimize resolution and accuracy: an innermost convection-allowing grid with a 2 km horizontal resolution (D03; depicted in Fig. 1, purple box), an intermediate grid at 6 km resolution (D02; Fig. 1, red box), and a stationary outer domain at 18 km resolution (D01; Fig. 1, outermost domain). The inner two domains, D02 and D03, are designed to move synchronously with the vortex, thereby ensuring that the TC is consistently within the domain of highest resolution. The spatial coverage of these domains is extensive, with D01 encompassing an area of approximately $77^\circ \times 77^\circ$ (288×576 grid points), D02 covering $27^\circ \times 27^\circ$ (304×604 grid points), and D03 spanning $7^\circ \times 8^\circ$ (265×472 grid points). These domains are laid out on a rotated latitude/longitude E-staggered grid and incorporate 61 vertical levels extending up to 2 hPa, thereby providing a comprehensive and detailed framework for analyzing TC dynamics (Biswas, 2018).

In our modeling approach, the convective processes within the two outer domains, which have resolutions of 18 km and 6 km, were parameterized using the simplified Arakawa–Schubert cumulus scheme, as outlined by Han and Pan (2006). However, in the innermost domain, with a finer 2 km grid spacing, these processes were simulated explicitly. The model also incorporated the Ferrier–Aligo microphysics scheme to simulate the impact of moist physical processes (Ferrier, 1994, 2005). Additionally, the model's physical schemes included an adaptation of the surface layer parameterization as proposed by Kwon et al. (2010) and the non-local planetary boundary layer parameterization scheme developed by Hong and Pan (1996). For radiation processes, the model utilized the Eta Geophysical Fluid Dynamics Laboratory longwave and shortwave radiation schemes, based on the foundational work of Schwarzkopf and Fels (1991) and Lacis and Hansen (1974). This

comprehensive suite of physics schemes (summarized in Table 1) was strategically selected to enhance the accuracy and reliability of the model in simulating the complex dynamics of TCs.

3. Experimental setup

3.1. Review of Typhoon Chan-hom

This study focuses on Typhoon Chan-hom, which developed in early October 2020. Typhoon Chan-hom initially intensified from a tropical depression to a tropical storm (TS) over the warm ocean southeast of Kagoshima, Japan, around 12 UTC on October 5, 2020. This moment marks the initial time for the forecasts depicted in Fig. 1. Subsequently, the typhoon moved northwestward. On October 8, Typhoon Chan-hom underwent a notable directional shift, veering sharply to the east near its peak intensity, and then proceeded northeastward off the eastern coast of Japan. This trajectory change is thought to be associated with the westward expansion and southward shift of the subtropical high (see Fig. 1). Moreover, the evolving dynamics of the upper-level trough and ridge to the north contributed to heightened uncertainties in the timing of Chan-hom's sharp turn. In the control run simulation, the storm turned too late, resulting in a modeled landfall in Japan, as illustrated by the blue and brown curves in Fig. 1(a–f). For more details about the information of Typhoon Chan-hom, refer to the best track data archive on <https://ncics.org/ibtracs/index.php?name=v04r00-2020277N21141>.

The considerable track forecast errors for Typhoon Chan-hom when comparing to the best track observation, which extended to several hundred kilometers, indicate a potentially low predictability for its trajectory (see blue and brown curves in Fig. 4). Additionally, the intensity forecasts in the control scenario, when compared with the best track observations, exhibited notable discrepancies. Specifically, there was an approximate error of 22 hPa in the minimum sea-level pressure (MSLP) and a 10 m s^{-1} error in the MSW speed at nearly a 96-h lead time, as shown in Fig. 6. These substantial errors in both track and intensity make Typhoon Chan-hom an apt case for investigating the impact of initial errors on the predictability of TC track and intensity.

Furthermore, the typhoon had an extended duration over open waters, lasting five to six days, without significant topographic influences (see the best track data archive on <https://ncics.org/ibtracs/index.php?name=v04r00-2020277N21141>). Throughout its lifetime, it sustained at least TS intensity for nearly seven days and intensified into a typhoon, with maximum sustained winds exceeding 40 m s^{-1} . This prolonged lifecycle, coupled with the high vortex intensity of Chan-hom, provides a unique opportunity to explore the potential temporal limits of TC predictability.

3.2. Definition of the regions where perturbations will be introduced

In our study, the primary objective was to explore the influence of region-specific initial uncertainties on the trajectory and intensity of TCs. To achieve this, we utilized the three nested domain framework to categorize the TC structure into distinct regions, as illustrated in Fig. 1 and detailed in Table 2. Initial ensemble perturbations would be superposed on individual domains as specified in Table 2 to initialize perturbed ensemble forecasts. The design of these domains are as follows. The innermost domain, designated as D03, encapsulates the TC's core¹ and the adjacent outer spiral rainbands, extending approximately 350 km from the TC center. This radius is nearly four times the RMW observed at the initial time (~ 90 km). The segment labeled as "part of D03" in Table 1 is particularly earmarked for examining the TC inner core (spanning 0–250 km) and the outer rainbands (250–350 km). This

¹ The inner core region of a strong TC generally includes the eye, eyewall, and the principle rain bands within about three times the radius of the maximum wind (Houze, 2010).

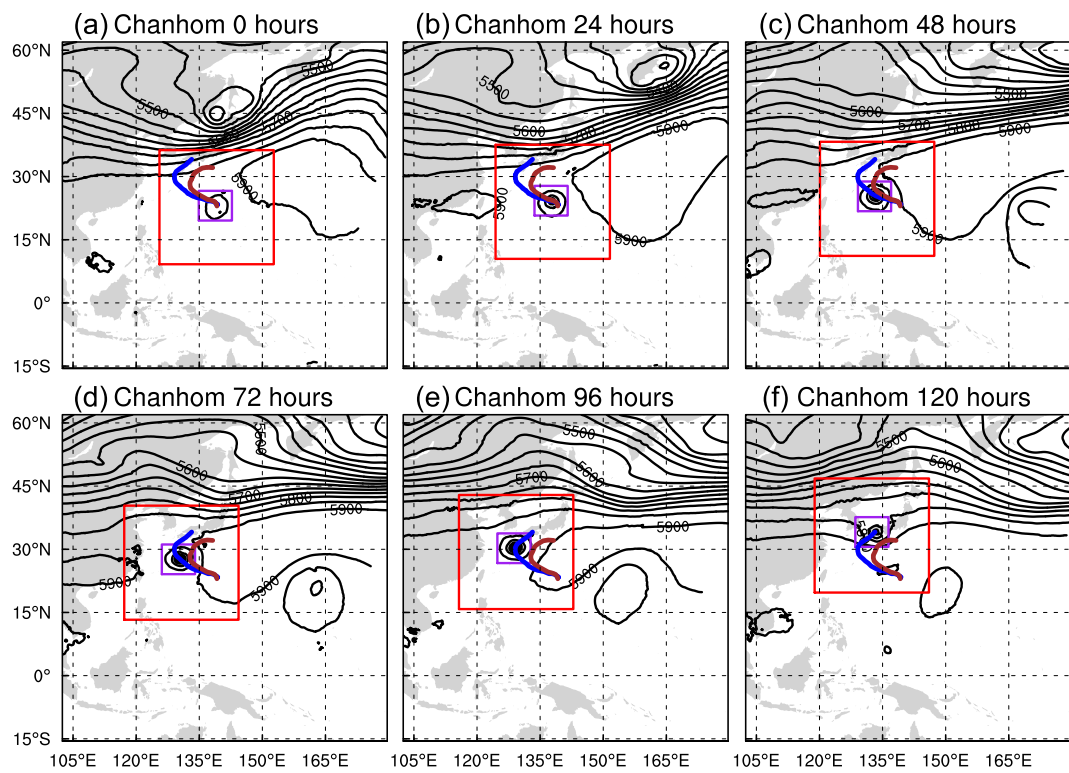


Fig. 1. Evolution of the 500 hPa geopotential height in D01 for (a–f) Typhoon Chan-hom during the control experiment from 0 to 120 h at intervals of 24 h overlain by the tracks of the control (dark blue) and best-track observations (brown) within the same time period. The red and purple squares highlight areas D02 and D03. (For interpretation of the references to colour in this figure legend, the reader is referred to the web version of this article.)

Table 1
A summary of the model physics schemes used in this study.

Cumulus parameterization	Microphysics	Surface process	Radiance process
Simplified Arakawa–Schubert scheme for D01 and D02, Han and Pan (2006) ; Not used for D03	Ferrier–Aligo scheme, Ferrier (1994, 2005)	An adaptation of the surface layer parameterization by Kwon et al. (2010) ; non-local planetary boundary layer parameterization scheme by Hong and Pan (1996)	Eta Geophysical Fluid Dynamics Laboratory longwave and shortwave radiation schemes (Schwarzkopf and Fels, 1991)

Table 2
Definitions of the regions in a tropical cyclone and their ranges and characteristics.

Region	Range (km)	Characteristics
D03	0–350	Inner core and outer rainbands
D03 to D02	350–1300	Near environment
D02 to D01	1300–3500	Far environment
Part of D03	0–250	Inner core
	250–350	Outer rainbands

segmentation, which includes both the inner core and outer rainbands, is in alignment with the definitions proposed by [Houze \(2010\)](#) and [Li and Wang \(2012\)](#). Furthermore, the region situated between the innermost (D03) and intermediate (D02) domains, encompassing a radius of about 350 to 1300 km, is identified as the near environment of the TC vortex. Lastly, the region lying between the intermediate (D02) and outer (D01) domains, extending from 1300 to 3500 km, corresponds to the area overlapping with synoptic-scale weather systems situated at a considerable distance from the TC center. This area is defined as the far

environment.

3.3. Experimental design

3.3.1. Generation of initial ensemble perturbations

[Fig. 2](#) presents a schematic diagram outlining our experimental methodology. The initial phase involves generating a control and twenty perturbed ensemble scenarios ($N = 20$), which are valid at the initial time point t_0 . These scenarios are created for the three nested domains within the HWRF model. The control and ensemble conditions at t_0 are derived from 6-h HWRF forecasts that span from t_{-1} to t_0 , all configured and set up identically.

For initialization at t_{-1} , we employ downscaled model fields from the control analysis of the Global Forecast System (GFS) at a resolution of 0.25° , along with perturbed analyses from the Global Ensemble Forecast System (GEFS) at a 0.5° resolution. These analyses are sourced from the National Centers for Environmental Prediction, as noted in [Zhou et al. \(2022\)](#). The forecasts from GFS and GEFS provide the lateral boundary conditions for the 6-h HWRF control (indicated by a red dashed arrow) and ensemble forecasts (indicated by a black dashed arrow), respectively.

Crucially, we utilize the 6-h short-term HWRF forecasts as the initial conditions at time t_0 , instead of directly using the fields in HWRF model domain downscaled from GFS/GEFS data. This approach is adopted to initiate the simulations with initial ensemble perturbations that are more dynamically evolved and spatially coherent after a 6-h spin-up. The 6-h spin-up time would weaken the possible influences from using global forecast data with different resolution for the HWRF control and ensemble forecasts. The rationale and effectiveness of this method are further illustrated in [Fig. 3](#), highlighting the advantage of starting with a more realistically evolved set of initial conditions for our simulations.

3.3.2. Superposition of region-specific initial perturbations

Following the establishment of the initial control and ensemble

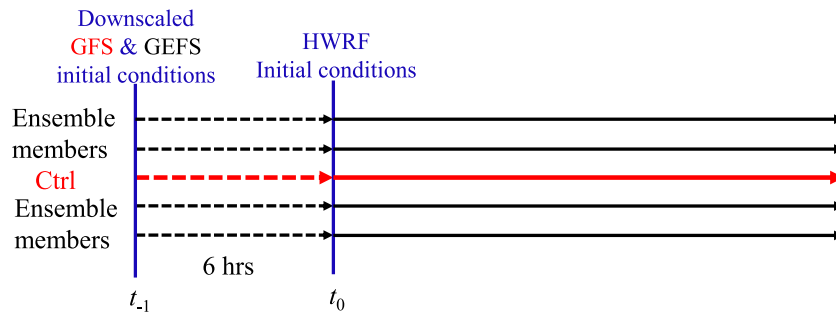


Fig. 2. Schematic diagram of the experimental flow. GFS, Global Forecast System; GEFS, Global Ensemble Forecast System.

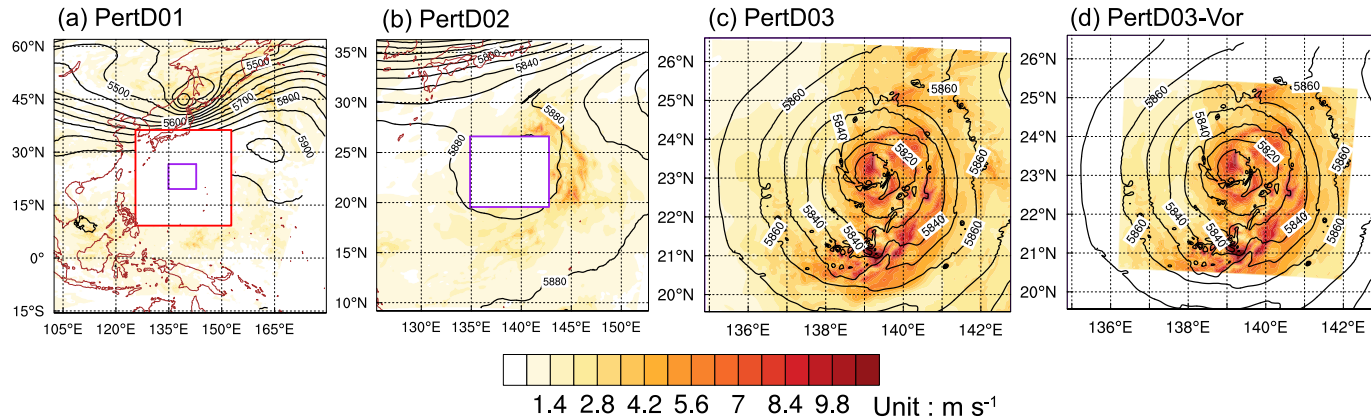


Fig. 3. Ensemble-averaged initial error amplitudes of the 500-hPa wind speed (shaded) in (a) D01 of PertD01, (b) D02 of PertD02, and D03 of (c) PertD03 and (d) PertD03-Vor overlaid by 500-hPa geopotential height (GH, contour) in Ctrl at the same time for Typhoon Chan-hom.

conditions for the HWRF model at time t_0 , the next step involves the design of numerical experiments. These experiments aim to assess the influence of region-specific initial errors on TC predictability. Based on the designated regions of TC structures, we structured the numerical experiments as detailed in Table 3. The baseline experiment, labeled as the “Ctrl” experiment (red solid arrow in Fig. 2), serves as the benchmark for the analysis of perturbed ensemble forecasts. In the Ctrl experiment, the forecast is initialized from the control initial condition at time t_0 without any perturbations on initial and boundary conditions. Experiment “PertD01” diverges from this baseline by employing a perturbed initial ensemble for the far environment of D01 (excluding the near environment, inner core, and outer rainbands), while maintaining identical initial conditions for D02 and D03 in the Ctrl experiment. Similarly, Experiment “PertD02” introduces perturbations in the near environment of D02, maintaining the initial conditions of D01 and D03 as in Ctrl. Experiment “PertD03” perturbs the regions of inner core and outer rainbands in D03 and D02, while the initial conditions in the remaining regions remain unchanged from those in the Ctrl experiment. To demonstrate the combined effect of initial errors in all these three domains, the experiment “PertD01D02D03” is also implemented in which D01, D02, and D03 are all perturbed.

To elucidate the distinct impacts of uncertainties within the inner core and outer rainbands of the TC, we conducted two additional experiments: “PertD03-Vor” and “PertD03-Rainb”. These experiments

involve initial perturbations focused on narrower regions compared to PertD03—specifically targeting the inner core and outer rainband areas, respectively. This suite of experiments (PertD01, PertD02, PertD03, PertD03-Vor, PertD03-Rainb, and PertD01D02D03) shares the same lateral boundary conditions as the Ctrl experiment, facilitating a clearer analysis of the effects stemming from initial condition errors. Lastly, Experiment “PertAll” encompasses all perturbations from the initial ensemble across the three nested domains and their lateral boundaries, offering a comprehensive view of the combined effects of these perturbations.

It should be noticed that perturbations superimposed in specified regions have the potential to induce physical and dynamical imbalances near the boundaries of these perturbations. Such imbalances can lead to the generation of spurious gravity waves (Ge et al., 2022), resulting in artificial error growth. To mitigate this adverse effect, a strategy is employed where, beyond the perturbed regions, the perturbed ensembles are gradually relaxed to the initial control state as implemented in Nystrom et al. (2018). This is achieved within an approximately 100-km transitional zone, utilizing a linear combination method to ensure a smooth transition.

Fig. 3 presents the ensemble-averaged amplitude of the initial perturbations in the 500-hPa wind speed across different domains: D01 of PertD01 (a), D02 of PertD02 (b), D03 of PertD03 (c) and PertD03-Vor (d). This figure highlights that the primary initial errors associated

Table 3
Descriptions of the control (Ctrl) and ensemble forecast experiments.

	Ctrl	PertD01	PertD02	PertD03	PertD03-Vor	PertD03-Rainb	PertD01D02D03	PertAll
D01 perturbed	No	Yes	No	No	No	No	Yes	Yes
D02 perturbed	No	No	Yes	No	No	No	Yes	Yes
D03 perturbed	No	No	No	Yes	Yes, vortex (0–250 km)	Yes, outer rainbands (250–350 km)	Yes	Yes
Boundary perturbed	No	No	No	No	No	No	No	Yes

with Typhoon Chan-hom are predominantly situated near the typhoon's eyewall, approximately 90 km from the center (as evidenced in Fig. 3c and d). Notably, an area of high perturbation magnitude within the typhoon's environment is identified near the East Asian trough, located north of the typhoon (Fig. 3a). The observed larger amplitude of initial perturbations in the typhoon's inner core, compared to its environment, can be attributed to distinct error growth dynamics. These dynamics are influenced by the intense meso- and convective-scale instability within the typhoon, as discussed by DeMaria (2009), in conjunction with the baroclinic environmental flow, as per Davis and Bosart (2003). The relative magnitude of initial perturbations in various designed regions might also potentially affect the sensitivity of TC forecast errors. However, this aspect was not considered in the present study. This is because the relative perturbation amplitude of the typhoon's inner core and environment, derived from the 6-h model evolution, mirrors the initial condition errors typically encountered in practical numerical weather prediction of TCs, as indicated by studies such as Ollinaho et al. (2021).

3.3.3. Control and perturbed ensemble forecasts

The third step is to execute the integration of both the initial control and ensemble conditions using the HWRF model from the initial time (t_0) across all experiments. This integration spanned a duration of five days with the output at intervals of 6 h. This approach contrasts with that of Judt et al. (2016), who employed stochastic perturbations in their model for ensemble generation. In this study, we compared perturbed ensemble forecasts with the Ctrl, as opposed to the truth (or analysis states). Given that all the ensemble and Ctrl forecasts were generated using the same model configuration and setup, this experimental design can be considered as an approximation of "an almost perfect procedure". This strategy is intentionally adopted to focus on illustrating the IE-predictability specific to TC. The chosen initial time t_0 corresponds to the moment when Typhoon Chan-hom escalated to TS intensity, reaching near 18 m s^{-1} , specifically at 1200 UTC on 5 October 2020.

4. IE-predictability of the TC track

Fig. 4 presents the five-day ensemble track forecasts for Typhoon Chan-hom (green curves) for four distinct experiments: PertD01 (Fig. 4a), PertD02 (Fig. 4b), PertD03 (Fig. 4c), and PertD03-Vor (Fig. 4d). These are overlaid with the typhoon tracks from both the Ctrl experiment and best track observations (blue and brown curves, respectively). It is important to note that these ensemble track forecasts are compared with those of the Ctrl experiment, rather than direct observations, in all subsequent analyses. This approach is adopted to more effectively highlight the impact of initial errors. As previously demonstrated in Fig. 1, the Ctrl experiment's track forecast for Typhoon Chan-hom exhibits significant discrepancies when compared to actual observations. The ensemble forecasts display a wide range of uncertainties, evident in their extensive spread which generally encompasses the

observed track, with the notable exception of the PertD01 experiment. This observation may suggest a relatively low inherent predictability for the track of Typhoon Chan-hom. Furthermore, the mean track difference between the ensemble forecasts and the control experiment shows remarkable variations across the different experiments, as further illustrated in Fig. 5a. These variations indicate the varying sensitivities of the experiments to the initial conditions and uncertainty regions.

Fig. 5 provides a detailed quantification of track errors for Typhoon Chan-hom, as well as the root-mean square error (RMSE) of the 500-hPa geopotential height in its near environment (specifically, from D03 to D02), as compared to the Ctrl forecast averaged across all ensemble members. In Fig. 5a, it is evident that the PertD03 simulation, which incorporates initial errors in D03, exhibits the largest track errors at all forecast lead times. This is followed by PertD02 and PertD01, which introduce initial errors in the near and far environments, respectively. Noticeably, when uncertainties in either the outer rainband (PertD03-Vor) or the inner core region (PertD03-Rainb) of the Typhoon are eliminated, there is a significant reduction in the mean track error of the Typhoon. This finding suggests a high sensitivity of the Typhoon's track to initial errors in D03, likely due to the complex interplay between errors in the inner core and those in the outer rainbands, which effectively serve as an interface with the surrounding environment.

Fig. 5b shows that the relative performance of track errors is consistent with the RMSE of the 500-hPa geopotential height within the near environment of the TC, thereby affirming that environmental steering predominantly dictates TC movement, as corroborated by most prior studies (George and Gray, 1976; Franklin et al., 1996; Galarneau and Davis, 2013). However, in the case of Typhoon Chan-hom, a notable interplay between errors in the inner core and outer rainbands appears to significantly influence and amplify the errors within the TC environment, leading to pronounced uncertainties in track forecasting. The markedly larger positional errors in the PertD03 and PertD03-Vor simulations, as compared to other experiments at day 0.25 and 0.5, can be attributed to the adjustment period needed to reconcile the imbalances between the inner TC structure, which contains errors, and the error-free surrounding environment despite the relaxation procedure used near the boundary. Beyond this initial transitional phase, PertD03 continues to exhibit a more rapid growth rate in track errors than PertD03-Vor. This suggests that the effects of stochastic perturbations at domain boundaries may have a transient and relatively insignificant impact on long-range track forecasts, compared to the perturbation development associated with physical processes within the TC.

5. IE-predictability of the TC intensity

5.1. Intensity uncertainty

This section delves into the analysis of forecast uncertainty related to the intensity of TCs, along with the corresponding error growth

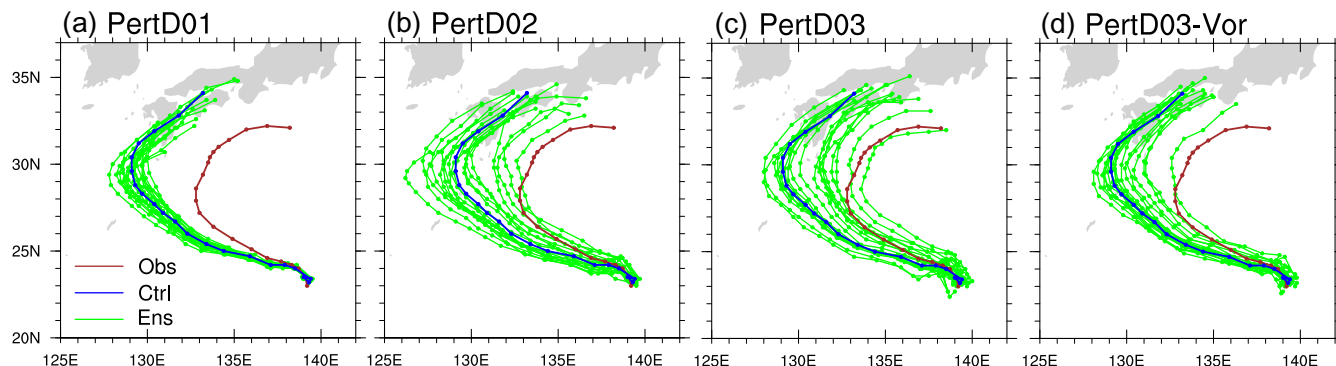


Fig. 4. Five-day tracks in the Ctrl forecast (dark blue), observations (brown), and the ensemble forecasts (green) of (a) PertD01, (b) PertD02, (c) PertD03, and (d) PertD03-Vor for Typhoon Chan-hom. (For interpretation of the references to colour in this figure legend, the reader is referred to the web version of this article.)

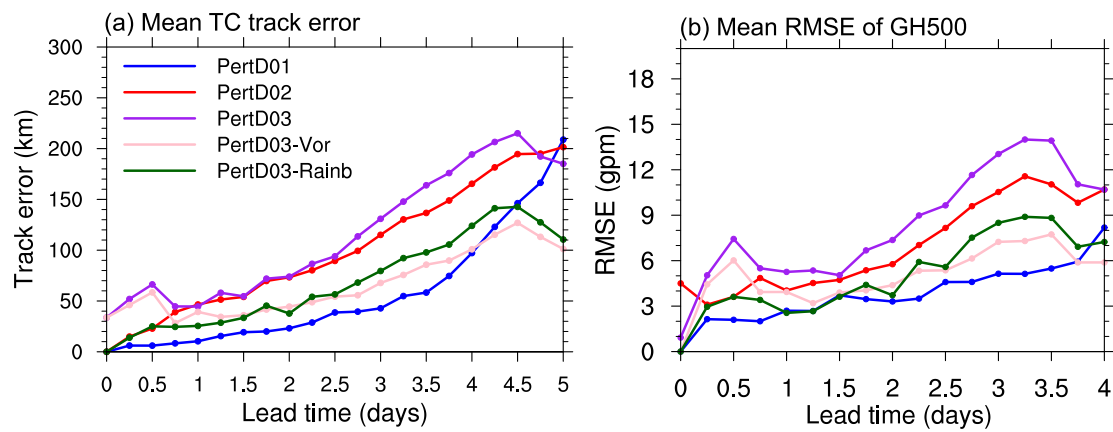


Fig. 5. Track errors and root-mean-square error of 500-hPa GH in near environment (i.e., D03 to D02) of the ensemble forecasts against the Ctrl forecast averaged over all ensemble members in PertD01 (dark blue), PertD02 (red), PertD03 (purple), PertD03-Vor (pink), and PertD03-Rainb (dark green) for Typhoon Chan-hom. (For interpretation of the references to colour in this figure legend, the reader is referred to the web version of this article.)

dynamics. The intensity of a TC is typically quantified using two primary metrics: the MSLP and the MSW. Fig. 6 presents the temporal evolution of both MSLP and MSW as observed in the ensemble forecasts, the Ctrl forecast, and the best track observations for Typhoon Chan-hom. An analysis of the Ctrl forecast (blue lines), when averaged over all lead times for Typhoon Chan-hom, reveals forecast errors of approximately 10 hPa in MSLP and 6 m s^{-1} in MSW, as compared to the observations. Echoing the pattern observed in the forecasts of TC track ensembles, the ensemble forecasts for TC intensity demonstrate varying degrees of spread across the different experiments. The specifics of these variations are discussed in further detail in the subsequent sections.

The ensemble-averaged typhoon intensity forecast errors for experiments PertD01, PertD02, PertD03, and PertD03-Vor in Fig. 6 are calculated and shown in Fig. 7. It is evident that PertD03 (purple) exhibits more substantial errors in both MSLP and MSW compared to PertD01 (blue), PertD02 (red), and PertD03-Rainb (cyan) within the initial 3-day period. Notably, the intensity forecast errors for PertD03 remain similar to those of PertD03-Vor during the first three days, both

of which preserve initial uncertainties in the inner core (cf. the pink and purple curves). These observations suggest that the uncertainty in TC intensity is more acutely affected by errors within the inner-core structures, within a 250 km radius (approximately three times the radius of maximum winds), than by errors in the outer rainbands or the broader TC environment. This inference aligns with the findings of Nystrom et al. (2018). Nevertheless, the impact of initial errors in the near-TC environment on the forecast intensity error may become increasingly significant for longer lead times (beyond three days). This amplification occurs when outer errors propagate into the inner core, even surpassing the magnitude of errors originating within the inner core itself (cf. the red and purple curves). Moreover, PertD02 (red) demonstrates greater uncertainties in TC intensity compared to PertD01 (dark blue), implying that the predictability of TC intensity is more significantly impacted by initial errors in the near environment than those in the far environment.

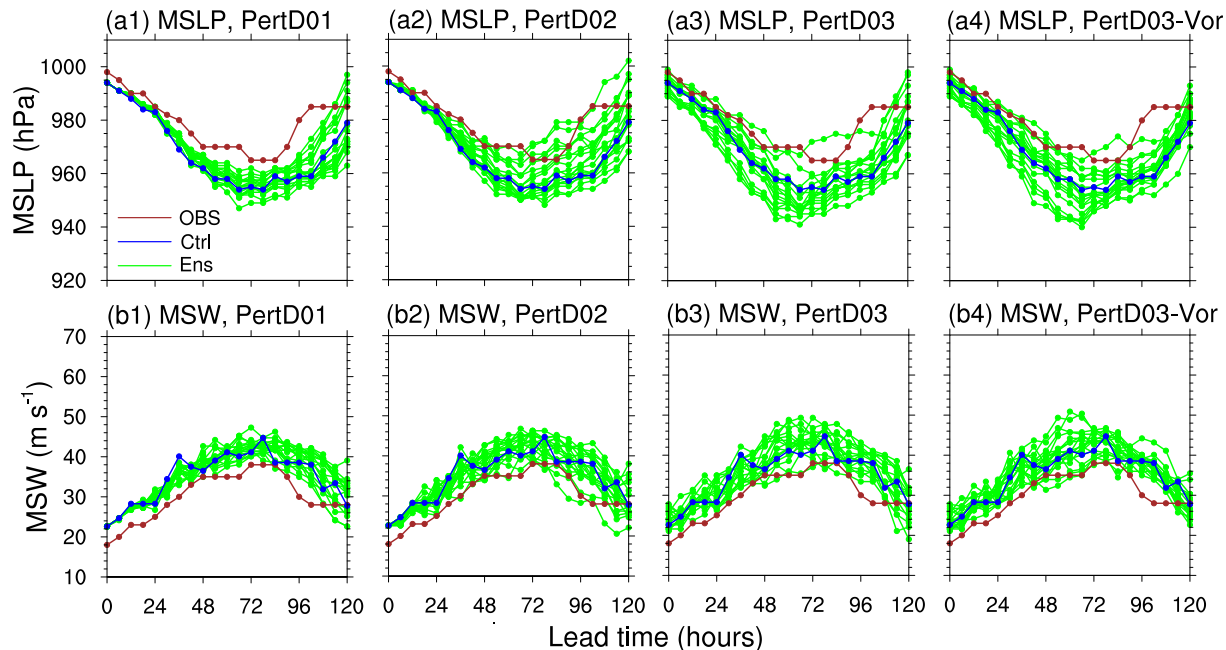


Fig. 6. Five-day (a) minimum sea-level pressure (MSLP) and (b) MSW in the Ctrl forecast (dark blue), observations (brown), and ensemble forecasts (green) of (a1, b1) PertD01, (a2, b2) PertD02, (a3, b3) PertD03, and (a4, b4) PertD03-Vor for Typhoon Chan-hom. (For interpretation of the references to colour in this figure legend, the reader is referred to the web version of this article.)

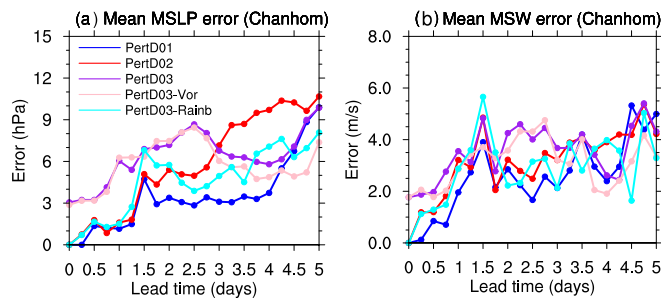


Fig. 7. Intensity errors of the ensemble forecasts against the Ctrl forecast averaged over all ensemble members in PertD01 (dark blue), PertD02 (red), PertD03 (purple), PertD03-Vor (pink), and PertD03-Rainb (cyan) in terms of the (a) MSLP and (b) MSW for Typhoon Chan-hom. (For interpretation of the references to colour in this figure legend, the reader is referred to the web version of this article.)

5.2. Scale-dependent error growth

Previous studies have shown that the evolution of TC intensity is intricately linked to both symmetrical and asymmetrical structures within the TC's inner core (Moller and Montgomery, 2000; Nolan et al., 2007; Yang et al., 2007; and Persing et al., 2013). To explore how initial errors within the TC impact intensity predictability, we employed a Fourier decomposition algorithm, akin to the approach used by Judt et al. (2016). This algorithm was applied to decompose the azimuthal structures of the 10-m wind amplitude field within a 300-km radius of the TC center. The decomposition of the original 10-m wind amplitude field within this radius yields the mean state (wave number 0) and 180 wave component fields, as illustrated in Fig. 8. According to the categorization by Judt et al. (2016), wave number 0 corresponds to the mean

vortex, and wave number 1 represents vortex-scale asymmetry. Wave numbers 2 through 5 are indicative of the structures akin to TC rain bands, while scales of wave numbers 6 and higher are associated with smaller mesoscale and convective features within the TC circulation.

Fig. 9 delineates the azimuthal mean error variances of the 10-m wind amplitude across different scales within the ensembles, analyzed over a 300-km radius from the TC center as a function of lead time for experiments PertD01 (a), PertD02 (b), and PertD03 (c). For comparative purposes, the temporal mean spectrum of twice the square of the 10-m wind amplitude at various scales from the Ctrl experiment in the same region is illustrated using black dashed lines. Points in time where the error variance surpasses this reference are considered as the limit of predictability for each respective scale. To clearly illustrate the error growth and the predictability limit, Fig. 9(d)-(f) further show the ratio of the mean error variance to the reference magnitude (i.e., colored solid lines vs. black dashed lines) for the first twenty wave numbers as a function of lead time. The corresponding limits of predictability are also highlighted with pink circles. In the case of Typhoon Chan-hom, it is evident that the mesoscale and convective scales (wave numbers ≥ 6) maintain predictability only up to 12 h when initial errors are introduced in the TC's near environment (PertD02) or inner-core regions (PertD03), as shown in Fig. 9b, c, e, and f. If the perturbations are confined to the far environment (PertD01), the predictability limit for scales with wave numbers 6 to 10 marginally extends to approximately 24 h, as illustrated in Fig. 9a and d.

Contrary to Judt et al. (2016), who posited that rainbands are predictable over a span of a few days with model stochastic perturbations, our findings suggest that the predictability of rainband scales at wave numbers 3–5 is confined to the initial 24 h when the inner-core region is perturbed (i.e., PertD03 in Fig. 9c and f). This discrepancy may possibly indicate differing impacts of initial and model-related uncertainties on the predictability of rainband-scale features. If the initial errors in the

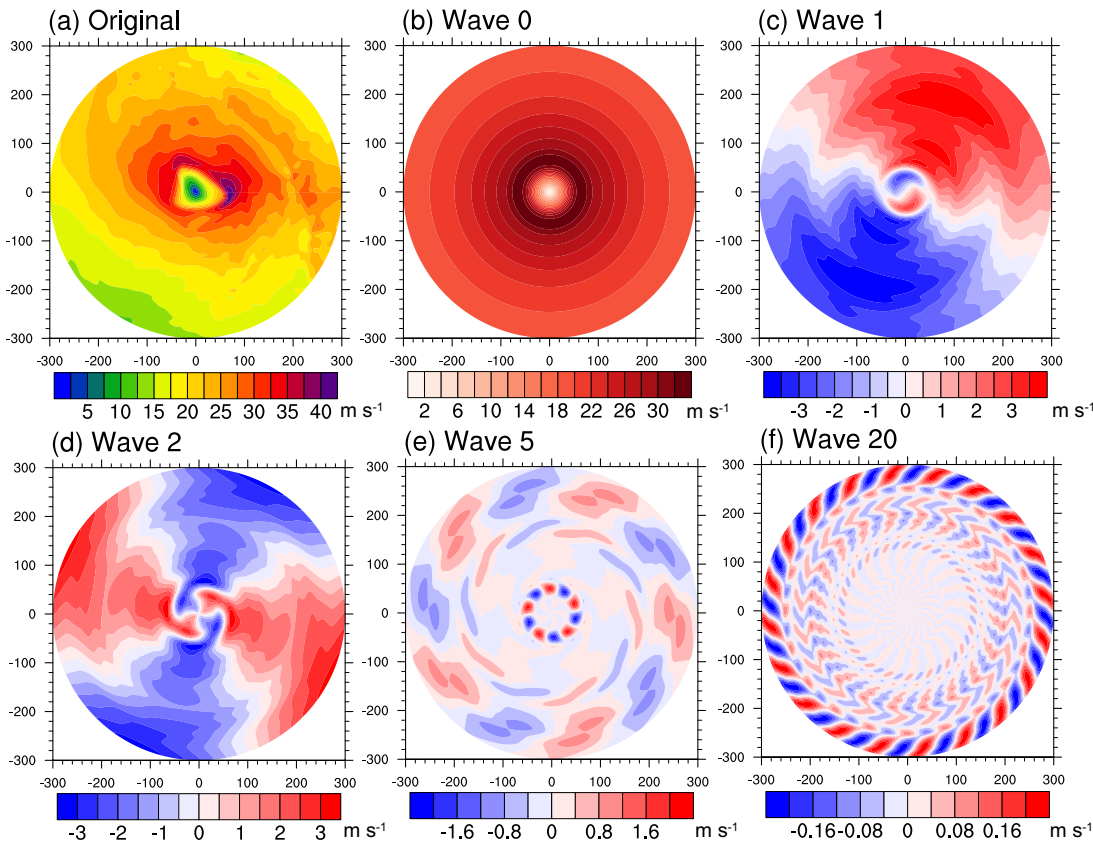


Fig. 8. (a) 10-m wind speed ($m s^{-1}$) in a 300-km radius from the TC center in the 2.25-day Ctrl forecast of Typhoon Chan-hom and its azimuthally decomposed components at wave numbers (b) 0, (c) 1, (d) 2, (e) 5, and (f) 20.

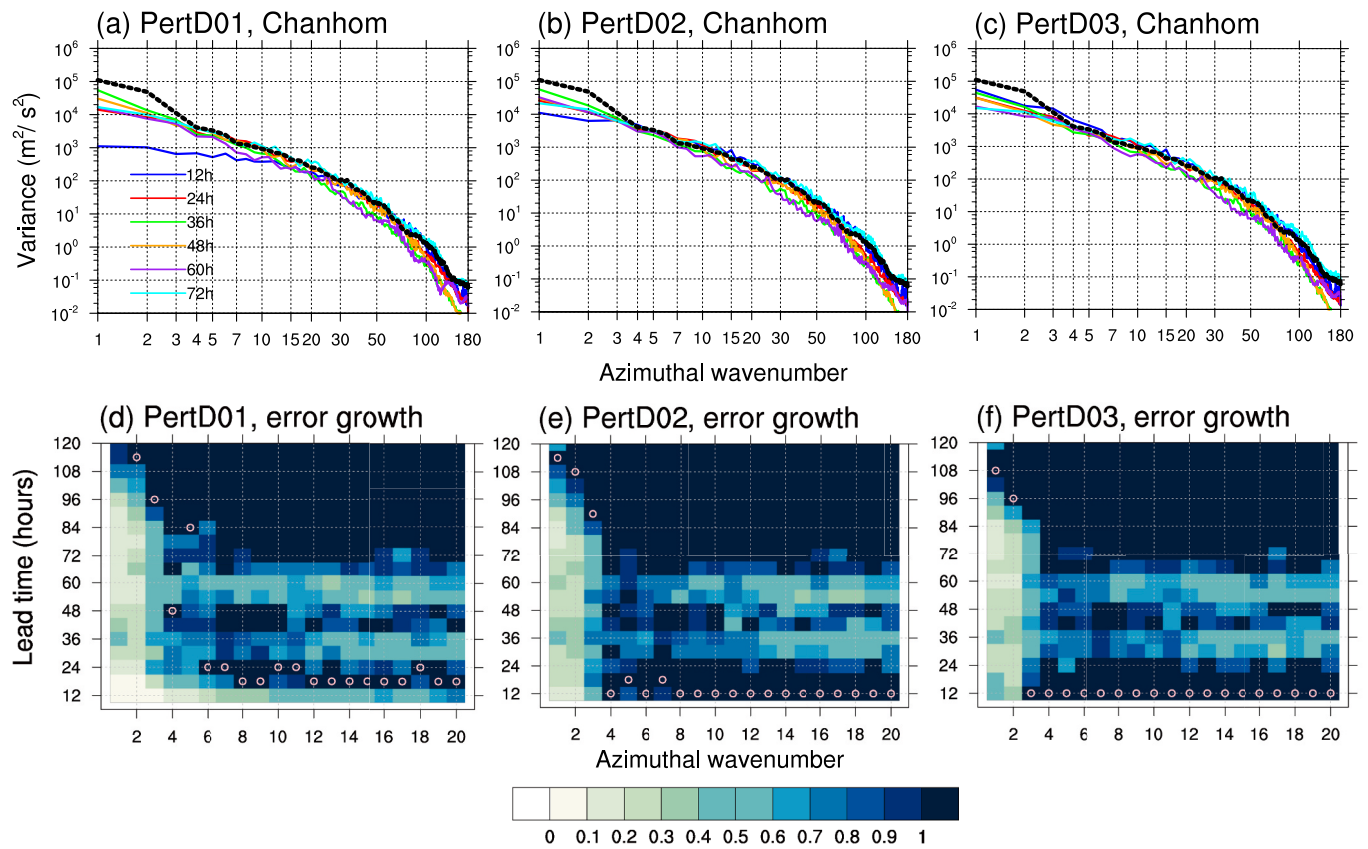


Fig. 9. Azimuthally mean and regionally integrated (0–300 km) error variances ($\text{m}^2 \text{s}^{-2}$) at different scales of the 10-m wind amplitude averaged over all ensemble members at different lead times for (a) PertD01, (b) PertD02, and (c) PertD03 of Typhoon Chan-hom. The temporal mean spectrum of twice the square of 10-m wind amplitude at different scales of the Ctrl experiment in the same region (black dashed lines) is shown as a reference. (d)–(f) are the ratios of error variances to the reference magnitude for waves 1–20 as a function of lead time for PertD01, PertD02, and PertD03. The corresponding predictability limits are highlighted with pink purples. (For interpretation of the references to colour in this figure legend, the reader is referred to the web version of this article.)

inner core and near environment of Chan-hom could be effectively eliminated, the predictability limit of features at rainband scales (wave numbers 3–5) may be extended to around three days (Fig. 9a and d). Our results align with those of Judt et al. (2016) regarding the mean flow of the TC (wave number 0; not shown) and major asymmetrical components (wave numbers 1–2). These components appear resistant to error propagation from smaller scales and remain predictable for a significantly longer duration, at least 4 days. Notably, once the perturbation variances surpass their scale's saturation level, they tend to fluctuate arbitrarily around the saturation reference, likely due to the limited sample size (Fig. 9a–c).

In Fig. 9a and c, we observe that the predictability of rainband scales with wave numbers 3–5 in Typhoon Chan-hom varies notably between the PertD01 and PertD03 experiments at the 12-h forecast lead time. Specifically, in PertD01, these scales remain predictable, whereas in PertD03, they become unpredictable within the same timeframe. This discrepancy necessitates a closer examination of the 12-h composite radar reflectivity in D03, which provides an approximate representation of the typhoon-induced rainfall as predicted by both the Ctrl and ensemble forecasts in PertD01 and PertD03 (see Fig. 10). Here, we present data from only three randomly selected ensemble members for clarity.

Fig. 10a reveals a distinct spiral rainfall pattern in the Ctrl experiment, stretching from the south to the east and northeast of Typhoon Chan-hom. This pattern is characterized by high radar reflectivity, predominantly exceeding 28 dBZ. Notably, two key areas of rainfall concentration are identified: the southern region, delineated by a purple rectangle, features a cluster of convective storms, while the eastern region, marked by a black rectangle, is distinguished by a long, narrow,

north-south oriented rainband.

Crucially, the PertD01 ensemble members (Fig. 10 b1–b3), which incorporate initial perturbations from the typhoon's distant environment, accurately capture both the position and structure of the eastern rainband and the convective rainfall at the 12-h mark (as evidenced by the shaded and black contours). Conversely, the PertD03 ensemble members (Fig. 10 c1–c3), which include initial perturbations from the typhoon's inner core, demonstrate significant deficiencies in forecasting the long eastern rainband. These deficiencies are manifested in considerable discrepancies in both the position and intensity of the rainband. Moreover, the representation of convective storms in the southern region of Typhoon Chan-hom within the PertD03 ensembles is either highly erratic or entirely misaligned compared to the Ctrl experiment. This comparison underscores the critical influence of initial errors within the typhoon's inner core on the predictability of its rainbands, effectively reducing the predictability limit to <12 h.

5.3. Source of predictability in the TC intensity

Fig. 9 illustrates a notable resilience in the wave numbers 0–2 of the 10-m wind amplitude against upscale error growth, in stark contrast to the rapid error escalation and eventual saturation observed at smaller scales. To probe the underlying factors contributing to the predictability of these lower wavenumber components, an additional experimental setup, termed PertD03-RndD01, was conducted. This experiment mirrors the PertD03 setup but introduces a novel modification: the initial conditions of the D01 domain in the ensemble forecasts are replaced with variable fields, which are downsampled from the GFS analysis at a different valid time. In the PertD03-RndD01 experiment, the D01

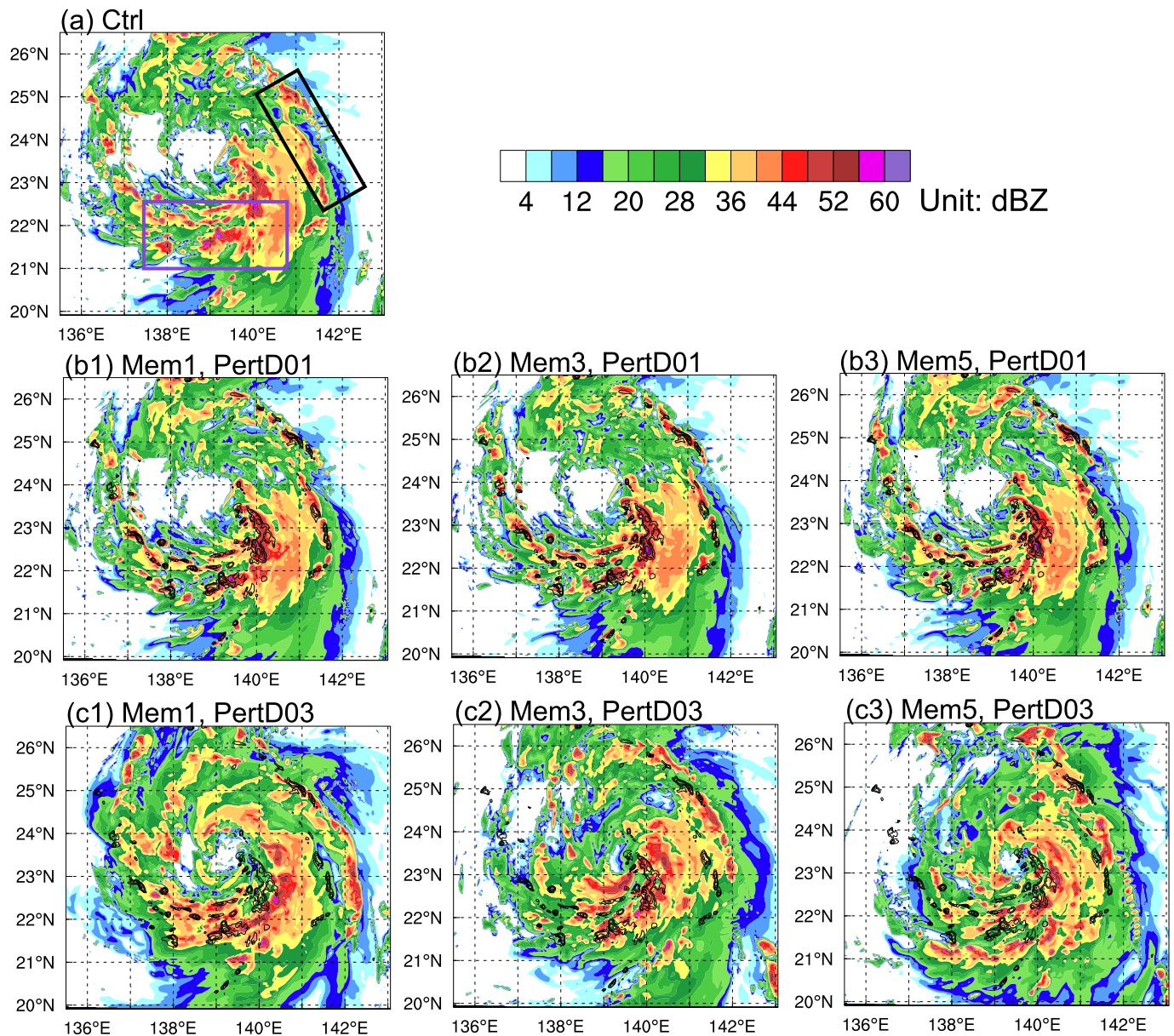


Fig. 10. Composite radar reflectivity (shaded) in D03 of in the 12-h (a) Ctrl and (b1–b3) ensemble forecasts of PertD01 and (c1–c3) PertD03. The composite radar reflectivity (≥ 44 dBZ) of the Ctrl experiment is shown as black contours in (b1–b3) and (c1–c3) for comparison.

domain for Typhoon Chan-hom employs a downscaled analysis based on data from 0000 UTC on 18 August 2020. This date is nearly two months removed from the initial start times of the experiment. The purpose of this experimental design is to examine the impact of the entirely unpredictable (or chaotic) far environment of the typhoon on its intensity predictability.

The analysis of the temporal evolution of error variance in the surface wind spectra within the TC's inner core, for the PertD03-RndD01 experiment (not shown), reveals that for wave numbers >2 , the error variance reaches saturation within <12 h, a finding that aligns with the observations from the PertD03 experiment as illustrated in Fig. 9c. However, a marked difference is observed in the error variances for wave numbers 1–2; They are much closer to the saturation levels in PertD03-RndD01 compared to PertD03. This observation suggests that the primary determinant of predictability for the surface wind components at wave numbers 1–2 lies in the synoptic-scale environment surrounding the typhoon. This inference aligns with the conclusions drawn by [Judt et al. \(2016\)](#), reinforcing the significance of the larger-scale

atmospheric conditions in influencing the predictability of these specific wave numbers.

Fig. 11 presents a detailed comparison of the 10-m wind speed field within a 300-km radius of the Ctrl experiment for Typhoon Chan-hom at 66 h (Fig. 11a), alongside its synthesized wind field for wave numbers 0–2 (Fig. 11b). For context, the composite surface wind of wave numbers 0–2 is also shown for the PertD03 and PertD03-RndD01 ensemble experiments (Fig. 11 c1–c5 and d1–d5, respectively). It is observed that the wave components 0–2 account for approximately 95% of the variance in the 10-m wind amplitude in the Ctrl experiment (Fig. 11a and b). Upon comparing the ensemble members of PertD03 with those of PertD03-RndD01, it is found that the former more accurately captures the composite surface wind structure of wave numbers 0–2 as seen in the Ctrl experiment. This is indicated by the shading and contours, with a mean spatial correlation coefficient of 0.94, which markedly surpasses the latter's correlation coefficient of 0.83. This finding is in line with the lower error variance at wave numbers 0–2 in PertD03 compared to PertD03-RndD01 (not shown).

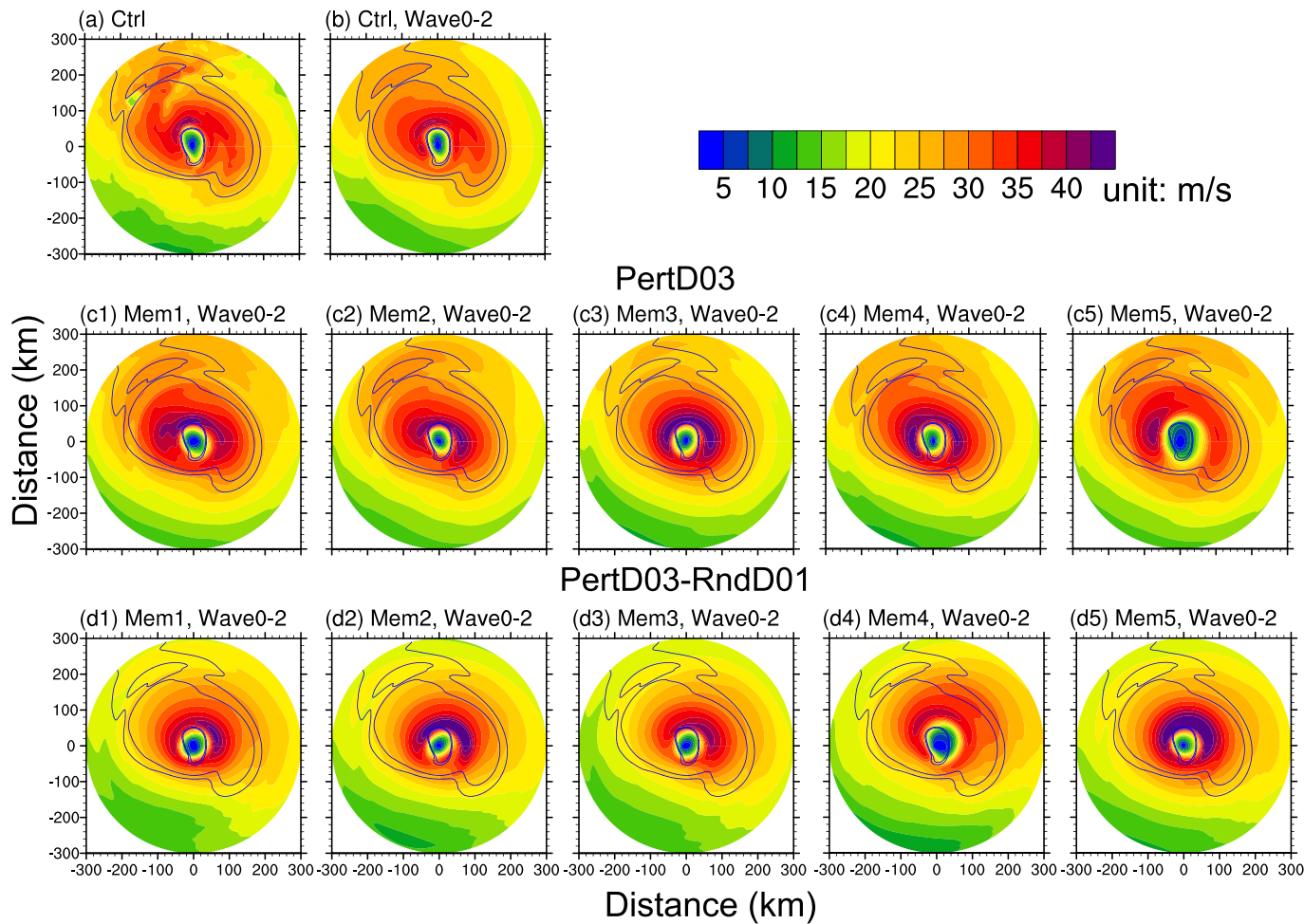


Fig. 11. (a) 10-m wind speed forecast (shading) in the 300-km radius of the Ctrl experiment at 66 h for Typhoon Chan-hom and (b) its composite wind field (shading) of wave numbers 0–2. (c1–c5) Composite 10-m wind speed fields (shading) of wave numbers 0–2 of the ensemble forecasts for PertD03 at 66 h. (d1–d5) are same as (c1)–(c5) but for PertD03-RndD01 at 66 h. Blue contours highlight wind speeds of 25 and 27.5 m s⁻¹ in the composite wind field of the Ctrl experiment in part (b). (For interpretation of the references to colour in this figure legend, the reader is referred to the web version of this article.)

The implication of these results is significant: they suggest that a decrease in the accuracy of the typhoon's surrounding environment correlates with a deterioration in the forecast quality of the vortex-scale asymmetric structures within the typhoon's inner core, specifically for wave numbers 0–2. This highlights the critical role of environmental precision in predicting the specific wind patterns within the inner core of a typhoon.

6. Combined effects of initial and lateral boundary perturbations on the TC predictability

In the realm of practical TC forecasting, uncertainties are inherent not only in the initial conditions but also in the boundary conditions of the forecasting models. This section delves into the cumulative impact of initial perturbations across all three nested domains (D01, D02, and D03) and boundary perturbations, collectively referred to as PertD01D02D03 and PertALL, respectively, on the predictability of both the track and intensity of TCs. Fig. 12 facilitates a comparative analysis between the ensemble-averaged forecast errors in TC track and intensity for the PertD01D02D03 and PertALL experiments and the experiment exhibiting the largest forecast errors among PertD01, PertD02, and PertD03. Specifically, PertD03 was identified as the least accurate in forecasting the track and intensity of Typhoon Chan-hom, as indicated by Figs. 5a and 7.

The comparison presented in Fig. 12 reveals that PertD01D02D03

yields higher forecast errors in both track and intensity than the experiments with initial errors confined to specific regions for Typhoon Chan-hom. Comparing the performance of PertD01D02D03 and PertALL, the boundary condition errors further increase the forecast errors of TC track and intensity. Moreover, the influence of boundary condition errors becomes noticeable beyond two-day lead time possibly when the advection effect from boundary condition errors reaches the near-TC environment and TC inner core. This observation suggests a significant decrease in predictability for both the track and intensity of the TC when the model accounts for all potential sources of uncertainties, encompassing both initial and boundary conditions. Essentially, this finding underscores the complex interplay of multiple sources of uncertainty in TC forecasting and their combined effect in exacerbating the challenges associated with predicting the path and strength of typhoons.

Fig. 13 displays the ensemble-averaged error variance spectrum of the 10-m wind amplitude within the inner core of Typhoon Chan-hom for the PertALL experiment. The temporal evolution of this error spectrum in PertALL exhibits similarities to that observed in PertD03, although PertALL demonstrates larger forecast errors in MSW as evidenced by the comparison in Fig. 12. Notably, the wind components corresponding to wave numbers 0–2 in PertALL retain predictability for at least three days as in PertD03. This observation indicates that these scales, deriving their predictability from the larger-scale TC environment, are pivotal in enabling skillful predictions of TC intensity for a period extending up to a few days.

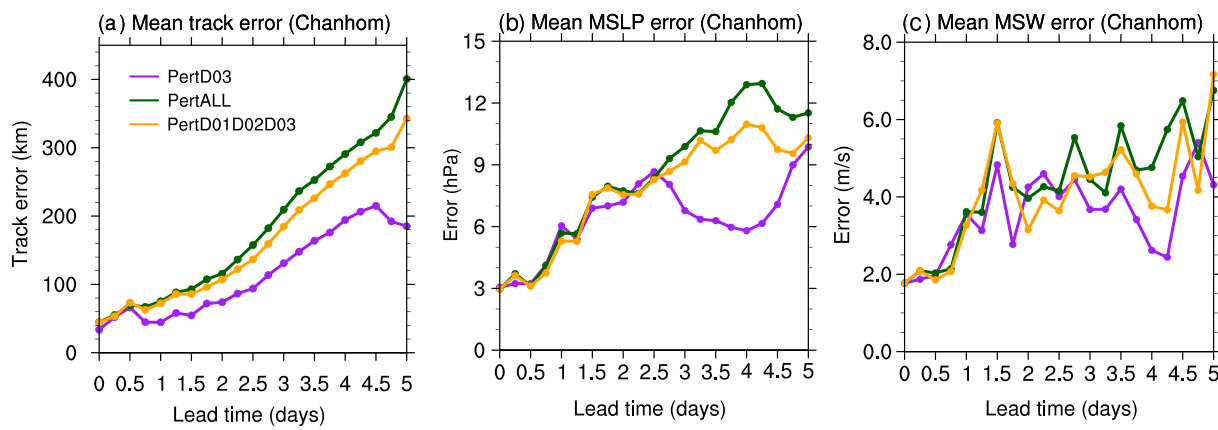


Fig. 12. Ensemble-averaged forecast errors of the (a) track, (b) MSLP, and (c) MSW for PertALL (dark green), PertD01D02D03 (orange), and PertD03 (purple) of Typhoon Chan-hom. (For interpretation of the references to colour in this figure legend, the reader is referred to the web version of this article.)

7. Conclusions and discussion

Understanding the predictability of tropical cyclones (TCs) is essential for enhancing the accuracy of their track and intensity forecasts. The concept of “initial condition error predictability” revolves around how initial errors amplify and influence predictions, providing an estimate of the highest achievable predictability. In this study, we evaluated the Initial-Error (IE) predictability of TC track and intensity. We accomplished this by comparing convection-allowing control forecasts with ensemble forecasts that incorporated perturbed initial conditions, utilizing the HWRF model. Our primary goal was to investigate how uncertainties in TC track and intensity respond to initial errors in various regions both inside and around the TC, shedding light on the accompanying error growth dynamics.

We employed a model configuration with three two-way nested domains (with resolutions of 18/6/2 km) to realistically simulate the scales and characteristics of TC inner cores and their surrounding environments. We designed experiments to investigate how initial errors in three key regions influence track and intensity predictability: (1) the far environment (1300–3500 km from the TC center), (2) the near environment (350–1300 km), and (3) the TC inner core and outer rainband regions (0–350 km). We selected Typhoon Chan-hom, a 2020 event in the western North Pacific Ocean characterized by significant uncertainties in both track and intensity, as a case study to demonstrate the sensitivity of TC forecasts to initial errors. Here, we present a summary of our key findings.

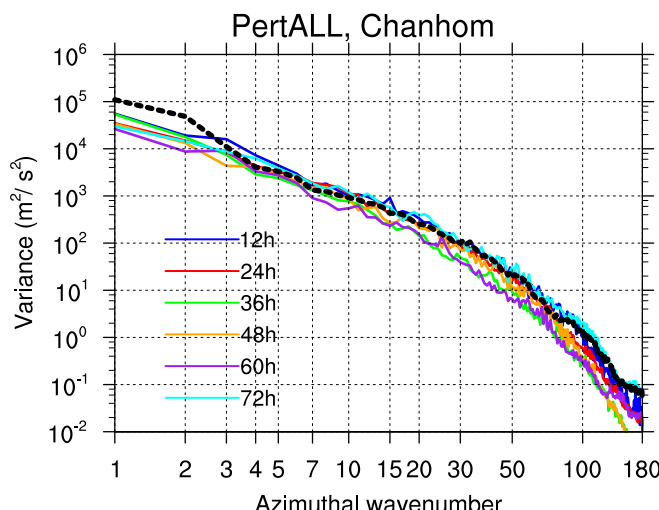


Fig. 13. Same as Fig. 9 but for PertALL.

- (1) In cases characterized by significant track errors, such as Typhoon Chan-hom, the most influential region for initial errors affecting TC track uncertainties is not always the broader environmental context but often the TC's internal structures. Specifically, the combined region encompassing the TC's inner core and outer rainbands (0–350 km) emerges as the most sensitive area. The pronounced interaction of initial errors within the TC's inner core and outer rainbands can result in heightened uncertainties within the TC's broader environment, subsequently degrading the accuracy of track forecasts (see Fig. 5b).
- (2) The region most responsive to initial errors regarding intensity uncertainties, particularly in the case of Typhoon Chan-hom, is the inner core region, spanning from 0 to 250 km. It's noteworthy that the intensity uncertainties triggered by initial perturbations in the TC's nearby environment surpass those arising from perturbations in the TC's more distant surroundings.
- (3) Our findings align with the conclusions drawn by Judt et al. (2016), who utilized model stochastic perturbations for ensembles. Specifically, we observe that errors at meso- and convective scales (wave numbers ≥ 6) within the TC inner core exhibit rapid growth, saturating within 12 h. However, our study diverges in terms of the rainband scales at wave numbers 3–5, which we find can only be reliably predicted up to 24 h when initial errors present in TC inner cores. This discrepancy may suggest that the influence of initial errors on the predictability of rainband-scale features differs from that of model-related errors.
- (4) The mean vortex and asymmetrical structures of the TC, characterized by wave numbers 1–2, maintain predictability for a minimum of four days owing to their dependence on the synoptic-scale environmental flow. However, it's essential to note that an accurate environmental flow alone may not guarantee improved predictions of Minimum Sea Level Pressure (MSLP) and Maximum Sustained Wind (MSW). These metrics are also influenced by highly turbulent and rapidly evolving finer-scale features with very short predictability. Hence, achieving a reasonable simulation of rainbands and smaller-scale structures within the TC inner core is critical for enhancing the accuracy of TC intensity forecasts.

While our study has analyzed the impact of region-dependent initial errors on TC track and intensity uncertainties and identified the most sensitive regions, the precise mechanisms by which initial errors in different regions induce uncertainties in TC track and intensity remain elusive. For instance, in the case of Typhoon Chan-hom with notable track errors, understanding the intensive interaction and influence of initial errors within the TC inner core and outer rainbands on the TC environment remains an open question. Additionally, elucidating the

physical processes responsible for uncertainties in TC intensity and inner-core structure at various scales requires further exploration in future research endeavors.

Open research

The global ensemble forecast product of GEFS at NCEP is downloaded from NCEP operational product inventory at <https://www.nco.ncep.noaa.gov/pmb/products/gens/>. The forecast product of the global forecast system (GFS) at NCEP is downloaded from <https://rda.ucar.edu/datasets/ds084.1/>. The Typhoon best-track data can be downloaded from the data archive center at <https://ncics.org/ibtracs/index.php?name=YearBasin-2020>

CRedit authorship contribution statement

Jie Feng: Conceptualization, Methodology, Software, Validation, Formal analysis, Investigation, Writing – original draft. **Falko Judt:** Methodology, Formal analysis, Investigation, Writing – review & editing. **Jing Zhang:** Methodology, Investigation, Writing – review & editing. **Xuguang Wang:** Investigation, Writing – review & editing.

Declaration of competing interest

The authors declare that they have no known competing financial interests or personal relationships that could have appeared to influence the work reported in this paper.

Data availability

Data will be made available on request.

Acknowledgments

The authors are grateful to Drs. Yuntao Wei and Guokun Dai at Fudan University, Dr. Deming Meng at Nanjing University, Prof. Tao Lian at the Second Institute of Oceanography, Profs. Wenjun Zhang, Xiefei Zhi, Qingqing Li, and Chao Wang at Nanjing University of Information Science and Technology in China for their input and helpful discussions. This study was supported by the National Natural Science Foundation of China (Grant No. 42288101, 42105054, and 42305060).

References

- Ashcroft, J., Schwendike, J., Griffiths, S.D., Ross, A.N., Short, C.J., 2021. The impact of weak environmental steering flow on tropical cyclone track predictability. *Q. J. R. Meteorol. Soc.* 147 (741), 4122–4142. <https://doi.org/10.1002/qj.4171>.
- Biswas, M.K., et al., 2018. Hurricane Weather Research and Forecasting (HWRF) Model: 2018 Scientific Documentation. Developmental Testbed Center, p. 112. http://www.dtcenter.org/sites/default/files/community-code/hwrf/docs/scientific_documents/HWRFv4.0a_ScientificDoc.pdf.
- Black, M.L., Gamache, J.F., Marks, J.D., Samsury, C.E., Willoughby, H.E., 2002. Eastern pacific Hurricanes Jimena of 1991 and Olivia of 1994: the effect of vertical shear on structure and intensity. *Mon. Weather Rev.* 130 (9), 2291–2312. [https://doi.org/10.1175/1520-0493\(2002\)130<2291:EPHJOA>2.0.CO;2](https://doi.org/10.1175/1520-0493(2002)130<2291:EPHJOA>2.0.CO;2).
- Cangialosi, J.P., Franklin, J.L., 2014. National Hurricane Center forecast verification report. http://www.nhc.noaa.gov/verification/pdfs/Verification_2013.pdf.
- Cangialosi, J.P., Blake, E., Demaria, M., Penny, A., Latto, A., Rappaport, E., Tallapragada, V., 2020. Recent progress in tropical cyclone intensity forecasting at the national hurricane center. *Weather Forecast.* 35 (5), 1913–1922. <https://doi.org/10.1175/WAF-D-20-0059.1>.
- Chen, S.S., Knaff, J.A., Marks, F.D., 2006. Effects of vertical wind shear and storm motion on tropical cyclone rainfall asymmetries deduced from TRMM. *Mon. Weather Rev.* 134 (11), 3190–3208. <https://doi.org/10.1175/MWR3245.1>.
- Chen, S.S., Price, J.F., Zhao, W., Donelan, M.A., Walsh, E.J., 2007. The CBLAST-Hurricane program and the next-generation fully coupled atmosphere-wave-ocean models for hurricane research and prediction. *Bull. Am. Meteorol. Soc.* 88 (3), 311–317. <https://doi.org/10.1175/BAMS-88-3-311>.
- Chen, S.S., Zhao, W., Donelan, M.A., Tolman, H.L., 2013. Directional wind-wave coupling in fully coupled atmosphere-wave-ocean models: results from CBLAST-hurricane. *J. Atmos. Sci.* 70 (10), 3198–3215. <https://doi.org/10.1175/JAS-D-12-0157.1>.
- Chia, H.H., Ropelewski, C.F., 2002. The interannual variability in the genesis location of tropical cyclones in the Northwest Pacific. *J. Clim.* 15 (20), 2934–2944. [https://doi.org/10.1175/1520-0442\(2002\)015<2934:TIVITG>2.0.CO;2](https://doi.org/10.1175/1520-0442(2002)015<2934:TIVITG>2.0.CO;2).
- Davis, C.A., Bosart, L.F., 2003. Baroclinically induced tropical cyclogenesis. *Mon. Weather Rev.* 131 (11), 2730–2747. [https://doi.org/10.1175/1520-0493\(2003\)131<2730:BITC>2.0.CO;2](https://doi.org/10.1175/1520-0493(2003)131<2730:BITC>2.0.CO;2).
- DeMaria, M., 2009. A simplified dynamical system for tropical cyclone intensity prediction. *Mon. Weather Rev.* 137 (1), 68–82. <https://doi.org/10.1175/2008MWR2513.1>.
- DeMaria, M., Sampson, C.R., Knaff, J.A., Musgrave, K.D., 2014. Is tropical cyclone intensity guidance improving? *Bull. Amer. Meteor. Soc.* 95, 387–398. <https://doi.org/10.1175/BAMS-D-12-00240.1>.
- Emanuel, K.A., 1986. An air-sea interaction theory for tropical cyclones. Part I: steady-state maintenance. *J. Atmos. Sci.* 43 (6), 585–604. [https://doi.org/10.1175/1520-0469\(1986\)043<0585:ASITFT>2.0.CO;2](https://doi.org/10.1175/1520-0469(1986)043<0585:ASITFT>2.0.CO;2).
- Emanuel, K., Zhang, F., 2016. On the predictability and error sources of tropical cyclone intensity forecasts. *J. Atmos. Sci.* 73 (9), 3739–3747.
- Emanuel, K., DesAutels, C., Holloway, C., Korty, R., 2004. Environmental control of tropical cyclone intensity. *J. Atmos. Sci.* 61 (7), 843–858. [https://doi.org/10.1175/1520-0469\(2004\)061<0843:ECOTCI>2.0.CO;2](https://doi.org/10.1175/1520-0469(2004)061<0843:ECOTCI>2.0.CO;2).
- Feng, J., Wang, X.G., 2019. Impact of assimilating upper-level dropsonde observations collected during the TCI field campaign on the prediction of intensity and structure of Hurricane Patricia (2015). *Mon. Weather Rev.* 147, 3069–3089.
- Feng, J., Wang, X.G., 2021. Impact of increasing horizontal and vertical resolution of the hurricane WRF model on the analysis and prediction of Hurricane Patricia (2015). *Mon. Weather Rev.* 149 (2), 419–441. <https://doi.org/10.1175/MWR-D-20-0144.1>.
- Feng, J., Qin, X., Wu, C., Zhang, P., Yang, L., Shen, X.S., Han, W., Liu, Y.Z., 2022. Improving typhoon predictions by assimilating the retrieval of atmospheric temperature profiles from the FengYun-4A's Geostationary Interferometric infrared Sounder (GIIRS). *Atmos. Res.* 280, 106391. ISSN 0169-8095. <https://doi.org/10.1016/j.atmosres.2022.106391>.
- Ferrier, B.S., 1994. A double-moment multiple-phase four-class bulk ice scheme. Part I: Description. *J. Atmos. Sci.* 51, 249–280. [https://doi.org/10.1175/1520-0469\(1994\)051<0249:ADMMPP>2.0.CO;2](https://doi.org/10.1175/1520-0469(1994)051<0249:ADMMPP>2.0.CO;2).
- Ferrier, B.S., 2005. An efficient mixed-phase cloud and precipitation scheme for use in operational NWP models. In: 2005 Spring Meeting, San Francisco, CA, Amer. Geophys. Union, Abstract A42A-02.
- Finocchio, P.M., Majumdar, S.J., 2017. The predictability of idealized tropical cyclones in environments with time-varying vertical wind shear. *J. Adv. Model. Earth Syst.* 9 (8), 2836–2862. <https://doi.org/10.1002/2017MS001168>.
- Franklin, J.L., Feuer, S.E., Kaplan, J., Aberson, S.D., 1996. Tropical cyclone motion and surrounding flow relationships: searching for beta gyres in omega dropwindsonde datasets. *Mon. Weather Rev.* 124, 64–84.
- Galarneau, T.J., Davis, C.A., 2013. Diagnosing forecast errors in tropical cyclone motion. *Mon. Weather Rev.* 141, 405–430. <https://doi.org/10.1175/MWR-D-12-00071.1>.
- Ge, Y., Lei, L., Whitaker, J.S., Tan, Z.M., 2022. The impact of incremental analysis update on regional simulations for Typhoons. *J. Adv. Model. Earth Syst.* 14 (10) <https://doi.org/10.1029/2022MS003084>.
- George, J.E., Gray, W.M., 1976. Tropical cyclone motion and surrounding parameter relationships. *J. Appl. Meteorol. Climatol.* 15, 1252–1264.
- Gopalakrishnan, S.G., Marks, F., Zhang, X., Bao, J.W., Yeh, K.S., Atlas, R., 2011. The experimental HWRF system: a study on the influence of horizontal resolution on the structure and intensity changes in tropical cyclones using an idealized framework. *Mon. Weather Rev.* 139 (6), 1762–1784. <https://doi.org/10.1175/2010MWR3535.1>.
- Hakim, G.J., 2013. The variability and predictability of axisymmetric hurricanes in statistical equilibrium. *J. Atmos. Sci.* 70 (4), 993–1005. <https://doi.org/10.1175/JAS-D-12-0188.1>.
- Han, J., Pan, H.-L., 2006. Sensitivity of hurricane intensity forecasts to convective momentum transport parameterization. *Mon. Weather Rev.* 134, 664–674. <https://doi.org/10.1175/MWR3090.1>.
- Hazelton, A., Alaka Jr., G.J., Fischer, M.S., Torn, R., Gopalakrishnan, S., 2023. Factors influencing the track of Hurricane Dorian (2019) in the West Atlantic: analysis of a HAFS ensemble. *Mon. Weather Rev.* 151 (1), 175–192.
- Hong, S.-Y., Pan, H.-L., 1996. Nonlocal boundary layer vertical diffusion in a medium-range forecast model. *Mon. Weather Rev.* 124, 2322–2339. [https://doi.org/10.1175/1520-0493\(1996\)124<2322:NBLVDI>2.0.CO;2](https://doi.org/10.1175/1520-0493(1996)124<2322:NBLVDI>2.0.CO;2).
- Houze, R.A., 2010, February. Clouds in tropical cyclones. *Mon. Weather Rev.* <https://doi.org/10.1175/2009MWR2989.1>.
- Houze, R.A., Chen, S.S., Lee, W.-C., Rogers, R.F., Moore, J.A., Stossmeister, G.J., Brodzik, S.R., 2006. The Hurricane rainband and intensity change experiment: observations and modeling of hurricanes Katrina, Ophelia, and Rita. *Bull. Am. Meteorol. Soc.* 87 (11), 1503–1522. <https://doi.org/10.1175/bams-87-11-1503>.
- Ito, K., Wu, C.C., 2013. Typhoon-position-oriented sensitivity analysis. Part I: Theory and verification. *J. Atmos. Sci.* 70 (8), 2525–2546. <https://doi.org/10.1175/JAS-D-12-0301.1>.
- Jayakrishnan, K.U., Kutty, G., George, B., 2020. On the predictability and dynamics of tropical cyclone: Nargis (2008). *J. Geophys. Res. Atmos.* 125 (9) <https://doi.org/10.1029/2019JD032040>.
- Judit, F., Chen, S.S., 2010. Convectively generated potential vorticity in rainbands and formation of the secondary eyewall in Hurricane Rita of 2005. *J. Atmos. Sci.* 67, 3581–3599.
- Judit, F., Chen, S.S., 2016. Predictability and dynamics of tropical cyclone rapid intensification deduced from high-resolution stochastic ensembles. *Mon. Weather Rev.* 144 (11), 4395–4420. <https://doi.org/10.1175/MWR-D-15-0413.1>.

- Judt, F., Chen, S.S., Berner, J., 2016. Predictability of tropical cyclone intensity: Scale-dependent forecast error growth in high-resolution stochastic kinetic-energy backscatter ensembles. *Q. J. R. Meteorol. Soc.* 142 (694), 43–57. <https://doi.org/10.1002/qj.2626>.
- Katz, R.W., Murphy, A.H., 2015. *Economic Value of Weather and Climate Forecasts*. Cambridge University Press, p. 240.
- Kieu, C.Q., Moon, Z., 2016. Hurricane intensity predictability. *Bull. Am. Meteorol. Soc.* 97 (10), 1847–1857. <https://doi.org/10.1175/BAMS-D-15-00168.1>.
- Kieu, C., Rotunno, R., 2022. Characteristics of tropical-cyclone turbulence and intensity predictability. *Geophys. Res. Lett.* 49 (8) <https://doi.org/10.1029/2021GL096544>.
- Kutty, G., Ghosh, K., 2017. The role of mid-level vortex in the intensification and weakening of tropical cyclones. *J. Earth Syst. Sci.* 126 (7) <https://doi.org/10.1007/s12040-017-0879-y>.
- Kwon, Y.C., Lord, S., Lapenta, B., Tallapragada, V., Liu, Q., Zhang, Z., 2010. Sensitivity of air-sea exchange coefficients (C_d and Ch) on hurricane intensity. In: 29th Conf. on Hurricanes and Tropical Meteorology. Amer. Meteor. Soc., Tucson, AZ, 13C.1. https://ams.confex.com/ams/29Hurricanes/techprogram/paper_167760.htm.
- Lacis, A.A., Hansen, J.E., 1974. A parameterization for the absorption of solar radiation in the earth's atmosphere. *J. Atmos. Sci.* 31, 118–133. [https://doi.org/10.1175/1520-0469\(1974\)031<0118:APFTAO>2.0.CO;2](https://doi.org/10.1175/1520-0469(1974)031<0118:APFTAO>2.0.CO;2).
- Li, Q., Wang, Y., 2012. A comparison of inner and outer spiral rainbands in a numerically simulated tropical cyclone. *Mon. Weather Rev.* 140 (9), 2782–2805. <https://doi.org/10.1175/MWR-D-11-00237.1>.
- Lorenz, E.N., 1969. The predictability of a flow which possesses many scales of motion. *Tellus* 21, 289–307. <https://doi.org/10.3402/tellusa.v21i3.10086>.
- Lu, X., Wang, X., Tong, M., Tallapragada, V., 2017. GSI-based, continuously cycled, dual-resolution hybrid ensemble-variational data assimilation system for HWRF: System description and experiments with edouard (2014). *Mon. Weather Rev.* 145 (12), 4877–4898. <https://doi.org/10.1175/MWR-D-17-0068.1>.
- Ma, Z., Fei, J., Liu, L., Huang, X., Li, Y., 2017. An investigation of the influences of mesoscale ocean eddies on tropical cyclone intensities. *Mon. Weather Rev.* 145 (4), 1181–1201. <https://doi.org/10.1175/MWR-D-16-0253.1>.
- Ma, Z., Fei, J., Huang, X., Cheng, X., 2018. Modulating effects of mesoscale oceanic eddies on sea surface temperature response to tropical cyclones over the Western North Pacific. *J. Geophys. Res. Atmos.* 123 (1), 367–379. <https://doi.org/10.1002/2017JD027806>.
- Moller, J.D., Montgomery, M.T., 2000. Tropical cyclone evolution via potential vorticity anomalies in a three-dimensional balance model. *J. Atmos. Sci.* 57 (20), 3366–3387. [https://doi.org/10.1175/1520-0469\(2000\)057<3366:TCEVPV>2.0.CO;2](https://doi.org/10.1175/1520-0469(2000)057<3366:TCEVPV>2.0.CO;2).
- Nolan, D.S., Moon, Y., Stern, D.P., 2007. Tropical cyclone intensification from asymmetric convection: energetics and efficiency. *J. Atmos. Sci.* 64 (10), 3377–3405. <https://doi.org/10.1175/JAS3988.1>.
- Nystrom, R.G., Zhang, F., Munsell, E.B., Braun, S.A., Sippel, J.A., Weng, Y., Emanuel, K., 2018. Predictability and dynamics of Hurricane Joaquin (2015) explored through convection-permitting ensemble sensitivity experiments. *J. Atmos. Sci.* 75 (2), 401–424. <https://doi.org/10.1175/JAS-D-17-0137.1>.
- Ollinaho, P., Carver, G.D., Lang, S.T.K., Tuppi, L., Eklblom, M., Järvinen, H., 2021. Ensemble prediction using a new dataset of ECMWF initial states-Open Ensemble 1.0. *Geosci. Model Dev.* 14 (4), 2143–2160. <https://doi.org/10.5194/gmd-14-2143-2021>.
- Persing, J., Montgomery, M.T., McWilliams, J.C., Smith, R.K., 2013. Asymmetric and axisymmetric dynamics of tropical cyclones. *Atmos. Chem. Phys.* 13 (24), 12299–12341. <https://doi.org/10.5194/acp-13-12299-2013>.
- Qin, X., Duan, W., Chan, P.W., Chen, B., Huang, K.N., 2023. Effects of Dropsonde Data in Field Campaigns on Forecasts of Tropical Cyclones over the Western North Pacific in 2020 and the Role of CNOP Sensitivity. *Adv. Atmos. Sci.* 40 (5), 791–803. <https://doi.org/10.1007/s00376-022-2136-9>.
- Qin, N., Wu, L., Liu, Q., 2021. Evolution of the moat associated with the secondary eyewall formation in a simulated tropical cyclone. *J. Atmos. Sci.* 78 (12), 4021–4035. <https://doi.org/10.1175/JAS-D-20-0375.1>.
- Qin, N., Wu, L., Liu, Q., Zhou, X., 2023. Driving forces of extreme updrafts associated with convective bursts in the eyewall of a simulated tropical cyclone. *J. Geophys. Res. Atmosph. (J. Geophys. Res.)* 128, e2022JD037061. <https://doi.org/10.1029/2022JD037061>.
- Ren, S., Lei, L., Tan, Z.M., Zhang, Y., 2019. Multivariate ensemble sensitivity analysis for super typhoon haiyan (2013). *Mon. Weather Rev.* 147 (9), 3467–3480. <https://doi.org/10.1175/MWR-D-19-0074.1>.
- Rios-Berrios, R., Torn, R.D., 2017. Climatological analysis of tropical cyclone intensity changes under moderate vertical wind shear. *Mon. Weather Rev.* 145, 1717–1738. <https://doi.org/10.1175/MWR-D-16-0350.1>.
- Rogers, R., 2010. Convective-scale structure and evolution during a high-resolution simulation of tropical cyclone rapid intensification. *J. Atmos. Sci.* 67 (1), 44–70. <https://doi.org/10.1175/2009JAS3122.1>.
- Schwarzkopf, M.D., Fels, S., 1991. The simplified exchange method revisited: an accurate, rapid method for computation of infrared cooling rates and fluxes. *J. Geophys. Res.* 96, 9075–9096. <https://doi.org/10.1029/89JD01598>.
- Selz, T., 2019. Estimating the intrinsic limit of predictability using a stochastic convection scheme. *J. Atmos. Sci.* 76 (3), 757–765. <https://doi.org/10.1175/JAS-D-17-0373.1>.
- Shapiro, L.J., Willoughby, H.E., 1982. The response of balanced hurricanes to local sources of heat and momentum. *J. Atmos. Sci.* 39 (2), 378–394. [https://doi.org/10.1175/1520-0469\(1982\)039<0378:TROBHT>2.0.CO;2](https://doi.org/10.1175/1520-0469(1982)039<0378:TROBHT>2.0.CO;2).
- Shin, S., Smith, R.K., 2008. Tropical-cyclone intensification and predictability in a minimal three-dimensional model. *Q. J. R. Meteorol. Soc.* 134 (636), 1661–1671. <https://doi.org/10.1002/qj.327>.
- Sippel, J.A., Zhang, F., 2008. A probabilistic analysis of the dynamics and predictability of tropical cyclogenesis. *J. Atmos. Sci.* 65 (11), 3440–3459. <https://doi.org/10.1175/2008JAS2597.1>.
- Sippel, J.A., Zhang, F., 2010. Factors affecting the predictability of Hurricane Humberto (2007). *J. Atmos. Sci.* 67 (6), 1759–1778. <https://doi.org/10.1175/2010JAS3172.1>.
- Sun, Y.Q., Zhang, F., 2016. Intrinsic versus practical limits of atmospheric predictability and the significance of the butterfly effect. *J. Atmos. Sci.* 73 (3), 1419–1438. <https://doi.org/10.1175/JAS-D-15-0142.1>.
- Tang, B., Emanuel, K., 2012. Sensitivity of tropical cyclone intensity to ventilation in an axisymmetric model. *J. Atmos. Sci.* 69 (8), 2394–2413. <https://doi.org/10.1175/JAS-D-11-0232.1>.
- Tao, D., Zhang, F., 2015. Effects of vertical wind shear on the predictability of tropical cyclones: practical versus intrinsic limit. *J. Adv. Model. Earth Syst.* 7 (4), 1534–1553. <https://doi.org/10.1002/2015MS000474>.
- Torn, R.D., Hakim, G.J., 2008. Ensemble-based sensitivity analysis. *Mon. Weather Rev.* 136, 663–677. <https://doi.org/10.1175/2007MWR2132.1>.
- Torn, R.D., Whitaker, J.S., Piegion, P., Hamill, T.M., Hakim, G.J., 2015. Diagnosis of the source of GFS medium-range track errors in Hurricane Sandy (2012). *Mon. Weather Rev.* 143 (1), 132–152. <https://doi.org/10.1175/MWR-D-14-00086.1>.
- Torn, R.D., Elless, T.J., Papin, P.P., Davis, C.A., 2018. Tropical cyclone track sensitivity in deformation steering flow. *Mon. Weather Rev.* 146 (10), 3183–3201. <https://doi.org/10.1175/MWR-D-18-0153.1>.
- Van Sang, N., Smith, R.K., Montgomery, M.T., 2008. Tropical-cyclone intensification and predictability in three dimensions. *Q. J. R. Meteorol. Soc.* 134 (632), 563–582. <https://doi.org/10.1002/qj.235>.
- Wang, Y., Wu, C.C., 2004, December. Current understanding of tropical cyclone structure and intensity changes - a review. *Meteorol. Atmos. Phys.* <https://doi.org/10.1007/s00703-003-0055-6>.
- Wu, L., Wang, B., Geng, S., 2005. Growing typhoon influence on East Asia. *Geophys. Res. Lett.* 32 (18), 1–4. <https://doi.org/10.1029/2005GL022937>.
- Wu, T.C., Liu, H., Majumdar, S.J., Velden, C.S., Anderson, J.L., 2014. Influence of assimilating satellite-derived atmospheric motion vector observations on numerical analyses and forecasts of tropical cyclone track and intensity. *Mon. Weather Rev.* 142 (1), 49–71. <https://doi.org/10.1175/MWR-D-13-00023.1>.
- Yang, B., Wang, Y., Wang, B., 2007. The effect of internally generated inner-core asymmetries on tropical cyclone potential intensity. *J. Atmos. Sci.* 64 (4), 1165–1188. <https://doi.org/10.1175/JAS3971.1>.
- Zhang, D.L., Chen, H., 2012. Importance of the upper-level warm core in the rapid intensification of a tropical cyclone. *Geophys. Res. Lett.* 39 (2) <https://doi.org/10.1029/2011GL050578>.
- Zhang, F., Tao, D., 2013. Effects of vertical wind shear on the predictability of tropical cyclones. *J. Atmos. Sci.* 70 (3), 975–983. <https://doi.org/10.1175/JAS-D-12-0133.1>.
- Zhang, H., Duan, W.S., Zhang, Y.C., 2023. Using the orthogonal conditional nonlinear optimal perturbations approach to address the uncertainties of tropical cyclone track forecasts generated by the WRF model. *Weather Forecast.* 38 (10), 1907–1933. <https://doi.org/10.1175/WAF-D-22-0175.1>.
- Zhang, B., Lindzen, R.S., Tallapragada, V., Weng, F., Liu, Q., Sippel, J.A., Bender, M.A., 2016. Increasing vertical resolution in US models to improve track forecasts of Hurricane Joaquin with HWRF as an example. *Proc. Natl. Acad. Sci. USA* 113 (42), 11765–11769. <https://doi.org/10.1073/pnas.1613800113>.
- Zhang, J.A., Rogers, R.F., Tallapragada, V., 2017. Impact of parameterized boundary layer structure on tropical cyclone rapid intensification forecasts in HWRF. *Mon. Weather Rev.* 145 (4), 1413–1426.
- Zhang, S., Pu, Z., Velden, C., 2018. Impact of enhanced atmospheric motion vectors on HWRF Hurricane analyses and forecasts with different data assimilation configurations. *Mon. Weather Rev.* 146 (5), 1549–1569. <https://doi.org/10.1175/MWR-D-17-0136.1>.
- Zhong, Q., Li, J., Zhang, L., Ding, R., Li, B., 2018. Predictability of tropical cyclone intensity over the Western North Pacific using the IBTrACS dataset. *Mon. Weather Rev.* 146 (9), 2741–2755. <https://doi.org/10.1175/MWR-D-17-0301.1>.
- Zhou, X., Zhu, Y., Hou, D., Fu, B., Li, W., Guan, H., Piegion, P., 2022. The development of the NCEP global ensemble forecast system version 12. *Weather Forecast.* 37 (6), 1069–1084. <https://doi.org/10.1175/waf-d-21-0112.1>.